VI International Conference on Computational Methods in Marine Engineering
MARINE 2015
F. Salvatore, R. Broglia and R. Muscari (Eds)

SIMULATION OF CONTACT BETWEEN SUBSEA PIPELINE AND TRAWL GEAR USING MORTAR-BASED ISOGEOMETRIC ANALYSIS

KJELL M. MATHISEN*†, KNUT M. OKSTAD‡, TROND KVAMSDAL‡ AND SIV B. RAKNES†

† Department of Structural Engineering
Norwegian University of Science and Technology, Trondheim, Norway
e-mail: kjell.mathisen@ntnu.no, siv.bente.raknes@ntnu.no

‡Department of Applied Mathematics
SINTEF Information and Communication Technology, Trondheim, Norway
e-mail: knut.morten.okstad@sintef.no, trond.kvamsdal@sintef.no

Key words: Isogeometric Analysis, NURBS, Contact Mechanics, Mortar Method, Large Deformation Plasticity, Pipeline, Pipe impact

Abstract. This paper focuses on the application of mortar-based isogeometric analysis to predict contact between subsea pipelines and trawl gear. The contact constraints are satisfied exactly with the augmented Lagrangian method, and treated with a mortar-based approach combined with a simplified integration method to avoid segmentation of the contact surfaces. The spatial discretization of the deformable body is performed with NURBS and C^0-continuous Lagrange polynomial elements. The numerical examples demonstrate that isogeometric surface discretization delivers more accurate and robust predictions of the response compared to Lagrange discretizations.

1 INTRODUCTION

Interaction between trawl gear from fishing vessels and subsea pipelines transporting oil and gas in the marine environment represents a crucial challenge for the co-existence of the fishing and offshore industry in many countries, and especially in Norway. In the near future the hydrocarbon exploitation is expected to take place in arctic waters where bottom trawling is even more appealing. The continuous development in the offshore industry necessitates regular updating of guidelines for design and corresponding computational strategies for simulation of the interference between pipelines and trawl gear. Initially extensive full-scale testing was carried out by the Norwegian Hydrodynamic Laboratory in Trondheim in a Norwegian joint industry project during the 1970s to study the interaction between trawl gear and pipelines [7, 4, 20]. Numerical methods for response

prediction of pipelines subjected to prescribed pull-over loads were introduced in a study carried out by Bergan and Mollestad [3, 19] in the early 1980s. More recently Igland and Søreide [13], Maalø *et al.* [18], Teigen *et al.* [24] and Longva *et al.* [15] have suggested far more refined strategies for estimating loads against pipelines due to trawl gear interaction.

Simulation of subsea pipeline and trawl gear interaction in general involves geometrical, material and contact nonlinearities, which need to be solved simultaneously. Non-smooth C^0-continuous finite element discretization techniques still constitute the most widely used approach in solving computational contact problems. In order to improve the performance of contact algorithms, various smoothing techniques have been proposed based on, e.g., Hermite C^1, Bézier and NURBS discretization of the contact surface. Although surface smoothing improves the evolution of the contact pressure, these approaches in general do not preserve consistency between volume and surface discretization. Within the framework of isogeometric analysis, which was introduced by Hughes *et al.* [11], smooth surface discretization can be achieved by representing the contact geometry by a NURBS surface that is directly inherited from the NURBS discretization of the volume.

The robustness of contact computations also depends on an accurate and smooth description of not only the contact geometry but also the contact pressure. It is well-known that node-to-surface (NTS) contact formulations are affected by several pathologies, and have been shown not to satisfy the contact patch test, which implies that mesh refinement does not necessarily increase the accuracy of the contact pressure. Several improvements to the NTS (or knot-to-surface, KTS, for isogeometric analysis) have been proposed, but they either do not satisfy the contact patch test or cause LBB-instability (Ladyzhenskaya-Babuska-Brezzi). However, the more recent mortar-based approaches constitute a method of consistently treating the global and local contact interaction, satisfying both the patch test and LBB-stability, albeit at a higher computational cost [2, 6, 8, 9, 10, 22].

The penalty (PL) method is the simplest and apparently the most widely used approach for solving contact problems. It leads to a pure displacement formulation where the constraints are enforced approximately. Furthermore, ill-conditioning may appear as the penalty parameter is increased in order to improve the satisfaction of the contact constraints. To avoid the drawbacks of the PL method, the augmented Lagrangian (AL) method may be adopted. There are two solution schemes commonly used in the context of the AL method. The so-called Uzawa method, which combines the AL regularization with a first-order update of the Lagrange multipliers [27]. Alternatively, a Newton-like solution scheme can be applied to solve the saddle-point problem for the displacements and Lagrange multipliers simultaneously as proposed by Alart and Curnier [1]. In view of the ascertained drawbacks of a non-mortar approach, we apply a mortar-based approach to satisfy the contact constraints combined with the latter version of the AL method, which is characterized by a remarkable degree of robustness and yields an asymptotic quadratic convergence rate in the Newton iterations. For comparison purposes, we have also implemented the PL method and C^0-continuous Lagrange polynomial elements.

In this paper mortar-based isogeometric analysis as formulated by De Lorenzis *et al.* [17] has been used to model a large deformation contact problem between a pipeline and trawl gear. The numerical example demonstrates that isogeometric surface discretizations deliver more accurate and robust predictions of the response compared to Lagrange discretizations. Experimental studies from Kristoffersen *et al.* [14] are used to validate the numerical results obtained for the interaction between the pipeline and trawl gear.

2 LARGE DEFORMATION CONTACT PROBLEM

This section gives a summary of the contact variables and the contact constraints within a continuum formulation of large deformation frictionless contact between two bodies. More details can be found in the monograph of Wriggers [27].

In this study finite deformation quasi-static frictionless contact problems will be considered in a purely mechanical setting. Consider two bodies $\mathcal{B}^i$, where the superscript $i = \{s, m\}$ denotes the slave (non-mortar) and master (mortar) bodies, respectively. The relation between the initial (reference) configuration $\mathbf{X}^i$, the displacement $\mathbf{u}^i$ and the current configuration $\mathbf{x}^i$ of a generic point of each body is given by

$$\mathbf{x}^i = \mathbf{X}^i + \mathbf{u}^i. \tag{1}$$

For modelling of contact between the two bodies $\mathcal{B}^s$ and $\mathcal{B}^m$, the contact interface denoted $\Gamma_c := \Gamma_c^s = \Gamma_c^m$ is pulled back to $\Gamma_{c0} := \Gamma_{c0}^s \neq \Gamma_{c0}^m$, where Γ_c^i and Γ_{c0}^i denote the contact boundary in the current and in the reference configuration of body $\mathcal{B}^i$, respectively. In the present formulation all contact integrals will be evaluated on Γ_{c0}^s. Defining $g_N = (\mathbf{x}^s - \mathbf{x}^m) \cdot \mathbf{n}^m$ to be the normal gap, λ_N the normal contact traction defined as the normal component of the interface Piola traction $\mathbf{t} := \mathbf{t}^m = -\mathbf{t}^s = \lambda_N \mathbf{n}^m$; the Kuhn-Tucker conditions for impenetrability on Γ_{c0} are

$$g_N \geq 0, \quad \lambda_N = \mathbf{t} \cdot \mathbf{n}^m \leq 0 \quad \text{and} \quad g_N \lambda_N = 0. \tag{2}$$

The frictionless contact problem between deformable elastic bodies can be formulated as a constrained minimization problem [27]:

$$\min_{\mathbf{u}} \Pi(\mathbf{u}) \quad \text{subject to} \quad g_N \geq 0 \quad \text{on} \quad \Gamma_c, \tag{3}$$

where $\Pi(\mathbf{u})$ is the potential energy.

In the PL method the contact constraints are enforced approximately

$$\lambda_N = \varepsilon_N \langle g_N \rangle_- \quad \text{where} \quad \langle g_N \rangle_- = \begin{cases} g_N, & g_N \leq 0, \\ 0, & g_N > 0, \end{cases} \tag{4}$$

where $\varepsilon_N > 0$ is the penalty parameter. Applying the above penalty regularization the constrained minimization problem may be transformed into an unconstrained minimization problem

$$\min_{\mathbf{u}} \Pi^{PL}(\mathbf{u}), \tag{5}$$

where the potential energy $\Pi(\mathbf{u})$ has been augmented by the following contact contribution to the virtual work

$$\delta\Pi_c^{PL} = \int_{\Gamma_{c0}} t_n \delta g_N d\Gamma. \tag{6}$$

δg_N denotes the variation of the normal gap.

For the solution of the constrained minimization problem we have adopted the AL method as formulated by Alart and Curnier [1]. In the AL method, a dual field of Lagrange multipliers λ_N is defined on the contact surface Γ_c, and the AL functional $\mathcal{L}$ is constructed as

$$\mathcal{L}(\mathbf{u}, \lambda_N) = \Pi(\mathbf{u}) + \int_{\Gamma_{c0}} l_n(g_N, \lambda_N) d\Gamma, \quad l_n(g_N, \lambda_N) = \begin{cases} \left(\lambda_N + \frac{\varepsilon_N}{2} g_N\right) g_N, & \hat{\lambda}_N \leq 0, \\ -\frac{1}{2\varepsilon_N} \lambda_N^2, & \hat{\lambda}_N > 0. \end{cases} \tag{7}$$

Here, $\varepsilon_N > 0$ is an arbitrary penalty parameter while the AL multiplier $\hat{\lambda}_N = \lambda_N + \varepsilon_N g_N$ is used to discriminate between contact ($\hat{\lambda}_N \leq 0$) and separation ($\hat{\lambda}_N > 0$). The main advantage of the AL method over the PL method and the Lagrange multiplier alternatives is that l_N and $\mathcal{L}$ are C^1-differentiable. Hence, the contact problem may now be reformulated as an unconstrained saddle-point problem

$$\min_{\mathbf{u}} \max_{\lambda_N} \mathcal{L}(\mathbf{u}, \lambda_N), \tag{8}$$

and the necessary condition of the saddle point takes the form

$$\delta\mathcal{L}(\mathbf{u}, \lambda_N) = \delta\Pi(\mathbf{u}) + \int_{\Gamma_{c0}} \left[\hat{\lambda}_N^{\text{eff}} \delta g_N + C_N \delta\lambda_N\right] d\Gamma = 0, \tag{9}$$

where the following notation has been introduced [17]

$$\hat{\lambda}_N^{\text{eff}} = \frac{\partial l_N}{\partial g_N} = \begin{cases} \hat{\lambda}_N, & \hat{\lambda}_N \leq 0, \\ 0, & \hat{\lambda}_N > 0, \end{cases} \qquad C_N = \frac{\partial l_N}{\partial \lambda_N} = \begin{cases} g_N, & \hat{\lambda}_N \leq 0, \\ -\frac{\lambda_N}{\varepsilon_N}, & \hat{\lambda}_N > 0. \end{cases} \tag{10}$$

The AL multiplier $\hat{\lambda}_N^{\text{eff}}$ is the state dependent normal contact traction, whereas C_N defines the constraints that are active depending on the contact state. Due to the C^1-differentiability of $\mathcal{L}$, continuity of both $\hat{\lambda}_N^{\text{eff}}$ and C_N is preserved as the contact state changes from contact to separation, hence upon discretization the resulting equations can be efficiently solved with Newton's method. Also note that in contrast to the PL method, for the AL method the contact constraints are enforced exactly regardless of the value of the penalty parameter, which can be kept conveniently low to improve the convergence behavior.

3 DISCRETIZATION WITH B-SPLINES AND NURBS

In order to overcome the problems with standard Lagrange discretization, the contact interfaces Γ_c^i and Γ_{c0}^i are discretized with NURBS surfaces that are directly inherited from NURBS volume discretization used for the solid body. This provides among others, the advantage of higher inter-element continuity within patches which ensures smooth surface representation without kinks between the elements. In what follows, some basic concepts for B-spline and NURBS curves, surfaces and volumes are briefly reviewed, the reader is referred to [5, 11, 21] for further details.

Geometrical objects are in general defined by explicit, implicit or parametric equations. *Non-uniform rational B-splines* (NURBS) curves, surfaces and volumes belong to the latter category, as they depend on a set of continuous parameters. NURBS are a generalization of B-splines and are constructed by projective transformation of B-spline basis functions. Contrary to the Lagrange basis functions that are local to elements, the B-spline parametric space is local to "patches". Patches are subdomains within which polynomial order of the basis functions and material parameters are assumed to be kept constant.

Univariate B-spline basis functions are defined by a *knot vector* Ξ, which is a set of non-decreasing parametric coordinates. The parameter space is the space where the basis functions are defined, and is partitioned into knot spans between the knots. The knot vector is written as:

$$\Xi = \{\xi_1, \xi_2, \ldots, \xi_{n+p+1}\}, \tag{11}$$

where ξ_i is the ith knot value, i is the knot index, $i = 1, 2, \ldots, n+p+1$, p is the polynomial order, and n is the number of basis functions. If a knot ξ_i is placed m_i times at the same location in the parametric space, the *multiplicity* of knot ξ_i is m_i, and the functions are C^{p-m_i} continuous at that location. If the knot vector has no repeated interior knots ξ_i, it defines $n - p$ non-zero knot spans (elements). If the knots are equally spaced; $\xi_{i+1} - \xi_i = \text{const.}, \forall i \in [1, n+p]$, the knot vector is said to be *uniform*, otherwise it is denoted as *non-uniform*. Furthermore Ξ is termed an *open* knot vector if the first and last entries have multiplicity $p+1$. In what follows we assume that Ξ is an open non-uniform knot vector.

B-spline basis functions for a given order are defined recursively by the Cox-de Boor recursion formula:

$$N_i^0(\xi) = \begin{cases} 1, & \text{if } \xi_i \leq \xi < \xi_{i+1}, \\ 0, & \text{otherwise,} \end{cases} \tag{12}$$

and

$$N_i^p(\xi) = \frac{\xi - \xi_i}{\xi_{i+p} - \xi_i} N_i^{p-1}(\xi) + \frac{\xi_{i+p+1} - \xi}{\xi_{i+p+1} - \xi_{i+1}} N_{i+1}^{p-1}(\xi), \quad \forall p \geq 1. \tag{13}$$

The order of the basis functions is equal to its polynomial degree, i.e. $p = 0, 1, 2, 3,$ etc., describes constant, linear, quadratic, cubic, etc., piecewise polynomials, respectively. The B-spline basis functions satisfy the following important properties:

1. Partition of unity: $\sum_{i=1}^{n} N_i^p(\xi) = 1, \ \forall \xi \in [\xi_1, \xi_{n+p+1}]$.
2. Local support: $\forall i$ the support of N_i^p is compact and contained in the interval $[\xi_i, \xi_{i+p+1}]$.
3. Non-negativeness: $N_i^p(\xi) \geq 0, \ \forall \xi \in [\xi_i, \xi_{i+p+1}]$.
4. Continuity: $\forall i$ each N_i^p is C^{p-m_i} continuous in the interval $[\xi_i, \xi_{i+p+1}]$.
5. Non-interpolatory: Except for the end knots or knots where the multiplicity $m_i = p-1$, $N_i^p(\xi_j) \neq \delta_{ij}$.
6. For $p = 0$ and $p = 1$, B-spline and Lagrange basis functions coincide.

A B-spline curve in $\mathbb{R}^{n_{sd}}$ can be expressed as a linear combination of the basis functions N_i^p with the spatial coordinates $\mathbf{P}_i$ of the *control points*:

$$\mathbf{C}(\xi) = \sum_{i=1}^{n} N_i^p(\xi)\mathbf{P}_i, \tag{14}$$

where n_{sd} denotes the number of spatial dimensions and $\mathbf{P}_i \in \mathbb{R}^{n_{sd}}$. What separates B-spline curves from curves constructed from a linear combination of the Lagrange basis functions with the nodal point coordinates, is that B-spline curves are related to a set of control point coordinates. These control points are the equivalent to the nodes, but B-spline curves will generally not pass through the control points.

NURBS curves can be constructed analogously to B-spline curves by replacing N_i^p with rational basis functions R_i^p:

$$\mathbf{C}(\xi) = \sum_{i=1}^{n} R_i^p(\xi)\mathbf{P}_i, \tag{15}$$

where the rational basis functions are obtained from a weighted linear combination of the B-spline functions by

$$R_i^p(\xi) = \frac{N_i^p w_i}{\sum_{j=1}^{n} N_j^p(\xi) w_j} = \frac{N_i^p w_i}{W(\xi)}. \tag{16}$$

where w_i is the weight associated with the ith control point $\mathbf{P}_i$. The weights normally have to fulfil the condition

$$w_i > 0 \ \forall i \in [1, n]\,. \tag{17}$$

As a NURBS curve does not necessarily interpolate control points, the weights can be used to influence the shape of the curve independently from the position of the control points. If the weights are increased, the curve approaches the shape of the control polygon, containing all the control points. While B-spline curves in general are not able to represent conic sections, by selecting appropriate values for the weights NURBS curves

may represent conic sections, like circles, exactly. Provided that all of the weight functions are unity, NURBS basis functions are identical to B-spline functions. Thus, NURBS inherits the fundamental properties of the B-spline basis functions.

We may extend the univariate B-spline and NURBS concepts to multiple dimensions with the use of tensor products. With n_{pd} parametric directions, for each parametric direction $d = 1, \ldots, n_{pd}$, we define an open non-uniform knot vector associated with the dth direction of a patch:

$$\Xi^d = \left\{\xi_1^d, \xi_2^d, \ldots, \xi_{n_d+p_d+1}^d\right\}, \tag{18}$$

Here, p_d is the polynomial order of the accompanying B-spline basis functions, ξ_i^d is the ith knot and n_d is the number of accompanying control points in the dth direction. Next, we define a multi-index $\boldsymbol{i} \in \mathbb{Z}^{n_{pd}}$ and the set

$$I = \left\{\boldsymbol{i} = \left\{i_1, \ldots, i_{n_{pd}}\right\} | i_d \in \{1, \ldots, n_d\}, d = 1, \ldots, n_{pd}\right\}. \tag{19}$$

A corresponding multi-index of polynomial orders and parametric coordinates are defined by

$$\boldsymbol{p} = \left\{p_1, \ldots, p_{n_{pd}}\right\} \quad \text{and} \quad \boldsymbol{\xi} = \left\{\xi^1, \ldots, \xi^{n_{pd}}\right\}. \tag{20}$$

For a given choice of $\boldsymbol{p}$, for each multi-index $\boldsymbol{i} \in I$, n_{pd}-dimensional NURBS basis functions can be obtained by tensor products of one-dimensional NURBS basis functions as follows:

$$R_{\boldsymbol{i}}^{\boldsymbol{p}}(\boldsymbol{\xi}) = \frac{w_{\boldsymbol{i}} B_{\boldsymbol{i}}^{\boldsymbol{p}}(\boldsymbol{\xi})}{\sum_{\boldsymbol{j} \in I} w_{\boldsymbol{j}} B_{\boldsymbol{j}}^{\boldsymbol{p}}(\boldsymbol{\xi})}, \tag{21}$$

where the n_{pd}-dimensional B-spline basis functions are obtained by

$$B_{\boldsymbol{i}}^{\boldsymbol{p}}(\boldsymbol{\xi}) = \prod_{d=1}^{n_d} N_{i_d}^{p_d}(\xi^d). \tag{22}$$

For a given control mesh, the corresponding NURBS surface and volume may now be defined analogously to the NURBS curve:

$$\mathbf{S}(\xi^1, \xi^2) = \sum_{i_1=1}^{n_1} \sum_{i_2=1}^{n_2} R_{i_1,i_2}^{p_1,p_2}(\xi^1, \xi^2) \mathbf{P}_{i_1,i_2}, \tag{23}$$

and

$$\mathbf{V}(\xi^1, \xi^2, \xi^3) = \sum_{i_1=1}^{n_1} \sum_{i_2=1}^{n_2} \sum_{i_3=1}^{n_3} R_{i_1,i_2,i_3}^{p_1,p_2,p_3}(\xi^1, \xi^2, \xi^3) \mathbf{P}_{i_1,i_2,i_3}. \tag{24}$$

Following the concept of isogeometric analysis [11], NURBS basis functions are used to discretize both the geometry in the reference and the current configuration and the unknown displacement field and its variation:

$$\mathbf{X} = \sum_{A=1}^{n_{cp}} R_A \mathbf{X}_A, \quad \mathbf{x} = \sum_{A=1}^{n_{cp}} R_A \mathbf{x}_A, \quad \mathbf{u} = \sum_{A=1}^{n_{cp}} R_A \mathbf{u}_A, \quad \text{and} \quad \delta\mathbf{u} = \sum_{A=1}^{n_{cp}} R_A \delta\mathbf{u}_A, \tag{25}$$

where $n_{cp} = \prod_{d=1}^{2} n_d$ is the number of control points associated with the contact surface (i.e. the product of the two parametric directions associated with the control surface), R_A is the two-dimensional NURBS basis function accompanying control point A, whereas $\mathbf{X}_A$, $\mathbf{x}_A$, $\mathbf{u}_A$ and $\delta\mathbf{u}_A$ are the corresponding reference coordinate, current coordinate, displacement and displacement variation vectors, respectively.

The above parameterization also applies to each individual knot span element of the contact surface:

$$\mathbf{X}^e = \sum_{a=1}^{n_e} R_a \mathbf{X}_a, \quad \mathbf{x}^e = \sum_{a=1}^{n_e} R_a \mathbf{x}_a, \quad \mathbf{u}^e = \sum_{a=1}^{n_e} R_a \mathbf{u}_a, \quad \text{and} \quad \delta\mathbf{u}^e = \sum_{a=1}^{n_e} R_a \delta\mathbf{u}_a, \tag{26}$$

where $n_e = \prod_{d=1}^{2}(p_d + 1)$ is the number of control points whose basis functions have support on a single knot span element of the corresponding contact surface.

Analogous interpolations are used for the Lagrange polynomial discretization, where standard Lagrangian basis functions and nodal points are used in place of NURBS basis functions and control points, respectively. In what follows, the above global and local parameterization will be applied by adding the superscript s and m for the slave and master contact surfaces, respectively.

4 CONTACT BETWEEN RIGID AND DEFORMABLE BODIES

For some simple analytical surfaces such as planar, cylindrical and spherical contact surfaces, the normal gap g_N may be determined in a closed form rather than iteratively by use of the closest point projection algorithm. For example the geometry of a rigid sphere is uniquely defined by its radius R and the coordinates of the center $\mathbf{x}^m \in \mathbb{R}^3$. In our work we assume that the rigid surface is the master surface Γ_c^m. Let $\mathbf{v}_n = \mathbf{x}^s - \mathbf{x}^m$, the normal gap g_N between a point $\mathbf{x}^s$ on the slave surface Γ_c^s and a corresponding point on the master surface Γ_c^m of a rigid sphere may then be computed directly by subtracting the radius R from $\|\mathbf{v}_n\|$:

$$g_N = \|\mathbf{x}^s - \mathbf{x}^m\| - R = \|\mathbf{v}_n\| - R = \sqrt{\mathbf{v}_n^T \mathbf{v}_n} - R. \tag{27}$$

By substituting the NURBS interpolations from Eq. (26) the expression for the variation of the normal gap on discretized form for the special case of a rigid spherical master surface become:

$$\delta g_N = \left[\sum_{a=1}^{n_e^s} R_a^s(\xi_s^1, \xi_s^2)\delta\mathbf{u}_a^s - \delta\mathbf{u}^m \right] \cdot \mathbf{n}^m, \tag{28}$$

where (ξ_s^1, ξ_s^2) are the parametric coordinates on Γ_{c0} and $\mathbf{n}^m$ denotes the outward normal of the rigid spherical master surface Γ_c^m pointing towards $\mathbf{x}^s$. Similar expressions may be derived for other simple analytical surfaces.

In order to formulate the variational problem in matrix form, it is convenient to introduce the following auxiliary vectors:

$$\delta\mathbf{u} = \begin{bmatrix} \delta\mathbf{u}_1^s \\ \vdots \\ \delta\mathbf{u}_{n_e^s}^s \\ \delta\mathbf{u}^m \end{bmatrix} \quad \text{and} \quad \mathbf{N} = \begin{bmatrix} R_1^s(\xi_s^1,\xi_s^2)\mathbf{n}^m \\ \vdots \\ R_{n_e^s}^s(\xi_s^1,\xi_s^2)\mathbf{n}^m \\ -\mathbf{n}^m \end{bmatrix}. \tag{29}$$

The expression for the variation of the normal gap may now be cast in a more compact matrix form

$$\delta g_N = \delta\mathbf{u}^T\mathbf{N} \tag{30}$$

5 MORTAR-BASED CONTACT FORMULATION

In order to relax the over-constrained knot-to-surface (KTS) contact formulation, a mortar approach may be applied. In this work, the original KTS contact constraints are relaxed based on the averaging of the normal gap penetration, as formulated in Tur *et al.* [26], Temizer *et al.* [25] and De Lorenzis *et al.* [16, 17]. Hence, the contact constraints are only enforced in an average sense at the control points and at the nodes with the NURBS and Lagrange discretizations, respectively. Like in Tur *et al.* [26], integration is in this work carried out without segmentation of the contact surfaces. In general this will introduce an error, which however can be reduced by increasing the number of quadrature points on the contact surface. In order to ensure a converged solution, $2p_d$ Gauss-Legendre quadrature points is employed in each direction d within each knot span element, see e.g. Hughes *et al.* [12] for a thorough discussion of efficient quadrature schemes appropriate for isogeometric analysis.

The mortar formulation implemented in this work for both the PL and the AL method is based on the approach presented by De Lorenzis *et al.* [16, 17]. For completeness, the main steps of the AL based mortar method is presented below.

With the mortar method, the contact contribution to the variation of the AL functional $\delta\mathcal{L}$, here denoted $\delta\Pi_c^{AL}$ becomes (see Eq. (9))

$$\delta\Pi_c^{AL} = \int_{\Gamma_{c0}} \left[\hat{\lambda}_N^{\text{eff}}\delta g_N + C_N\delta\lambda_N\right] d\Gamma = \sum_{A=1}^{n_{cp}^s} (\hat{\lambda}_{NA}^{\text{eff}}\delta g_{NA} + C_{NA}\delta\lambda_{NA})A_A, \tag{31}$$

where A_A denote the area of "competence"

$$A_A = \int_{\Gamma_{c0}} R_A d\Gamma, \tag{32}$$

and

$$\hat{\lambda}_{NA}^{\text{eff}} = \begin{cases} \hat{\lambda}_{NA} = \lambda_{NA} + \varepsilon_N g_{NA}, & \hat{\lambda}_{NA} \le 0, \\ 0, & \hat{\lambda}_{NA} > 0, \end{cases} \qquad C_{NA} = \begin{cases} g_{NA}, & \hat{\lambda}_{NA} \le 0, \\ -\frac{1}{\varepsilon_N}\lambda_{NA}, & \hat{\lambda}_{NA} > 0, \end{cases} \tag{33}$$

are the control point counterparts of the nominal AL multiplier $\hat{\lambda}_N^{\text{eff}}$ and contact constraint C_N, respectively.

Note that, contrary to the mortar formulation based on the PL method, the summation is here extended to all control points, and not only the active ones (i.e. those with $\hat{\lambda}_{NA} \leq 0$).

The main difference of the mortar formulation from the standard KTS, or node-to-surface (NTS) for Lagrange discretization, is the definition of the normal gap. The control point normal gap is defined as the weighted average of the corresponding "local" normal gaps with the basis functions as weights

$$g_{NA} = \frac{1}{A_A} \int_{\Gamma_{c0}} R_A \, g_N d\Gamma. \tag{34}$$

The variation of the control point normal gap is defined analogously

$$\delta g_{NA} = \frac{1}{A_A} \int_{\Gamma_{c0}} R_A \delta g_N d\Gamma. \tag{35}$$

The above definitions of the control point quantities substituted into Eq. (31) yields

$$\delta \Pi_c^{AL} = \sum_{A=1}^{n_{cp,a}^s} (\hat{\lambda}_{NA} \int_{\Gamma_{c0}} R_A \delta g_N d\Gamma + \delta \lambda_{NA} \, g_{NA} A_A) - \frac{1}{\varepsilon_N} \sum_{A=1}^{n_{cp,i}^s} \delta \lambda_{NA} \lambda_{NA} A_A, \tag{36}$$

where $n_{cp,a}^s$ and $n_{cp,i}^s$ define number of active and inactive control points, respectively (i.e. those with $\hat{\lambda}_{NA} \leq 0$ and $\hat{\lambda}_{NA} > 0$, respectively).

Next, we define $\hat{\lambda}_{NI}$ to be the interpolated value of the AL multiplier over the active control points

$$\hat{\lambda}_{NI} = \sum_{A=1}^{n_{cp,a}^s} \hat{\lambda}_{NA} R_A. \tag{37}$$

Substituted into Eq. (31) yields

$$\delta \Pi_c^{AL} = \int_{\Gamma_{c0}} \hat{\lambda}_{NI} \delta g_N d\Gamma + \sum_{A=1}^{n_{cp,a}^s} \delta \lambda_{NA} \, g_{NA} A_A - \frac{1}{\varepsilon_N} \sum_{A=1}^{n_{cp,i}^s} \delta \lambda_{NA} \lambda_{NA} A_A. \tag{38}$$

Let $\delta \boldsymbol{\lambda}$ and $\mathbf{N}_\lambda$ denote the vector of the variation of the control point Lagrange multiplier unknowns and the accompanying residuals

$$\delta \boldsymbol{\lambda} = \begin{bmatrix} \delta \lambda_1 \\ \vdots \\ \delta \lambda_{n_{cp}} \end{bmatrix} \quad \text{and} \quad \mathbf{N}_\lambda = \begin{bmatrix} N_{\lambda_1} \\ \vdots \\ N_{\lambda_{ncp}} \end{bmatrix} \tag{39}$$

where

$$N_{\lambda_A} = \begin{cases} g_{NA} A_A, & \hat{\lambda}_{NA} \leq 0, \\ -\frac{1}{\varepsilon_N} \lambda_{NA} A_A, & \hat{\lambda}_{NA} > 0. \end{cases} \tag{40}$$

Collecting the unknown control point displacements $\mathbf{u}$ and the control point Lagrange multiplier unknowns $\boldsymbol{\lambda}$ in the vector $\mathbf{z}$

$$\mathbf{z} = \begin{bmatrix} \mathbf{u} \\ \boldsymbol{\lambda} \end{bmatrix}, \tag{41}$$

and substituting the definitions in Eq. (29) and (39) into Eq. (38) yields

$$\delta \Pi_c^{AL} = \delta \mathbf{u}^T \int_{\Gamma_{c0}} \hat{\lambda}_{NI} \mathbf{N} d\Gamma + \delta \boldsymbol{\lambda}^T \mathbf{N}_\lambda = \delta \mathbf{z}^T \mathbf{R}, \tag{42}$$

where $\mathbf{R}$ denote the expression of the residual for the Newton-Raphson iterative scheme

$$\mathbf{R} = \begin{bmatrix} \mathbf{R}_u \\ \mathbf{R}_\lambda \end{bmatrix} = \begin{bmatrix} \int_{\Gamma_{c0}} \hat{\lambda}_{NI} \mathbf{N} d\Gamma \\ \mathbf{N}_\lambda \end{bmatrix}. \tag{43}$$

In order to solve the nonlinear equations a consistent linearization of the above expressions must be conducted to obtain the consistent tangent stiffness.

6 NUMERICAL RESULTS

The purpose of the numerical study is to compare and validate the presented mortar-based isogeometric contact model for numerical simulation of interaction between pipeline and trawl gear against experimental results. The experiments used for validation includes an extensive program of laboratory material and component testing carried out by Kristoffersen *et al.* [14]. A schematic sketch of the experimental setup is shown in Figure 1 [14]. In our study quasi-static simulations have been applied to simulate contact between the indenter and the pipe. This represents a simplification of the loading sequence and do not account for for any dynamic effects whatsoever.

The impact is modelled by prescribing the vertical displacement of the indenter (a rigid cylinder) downward ($d_I = 150$ mm). The pipe is made from X65 steel, a material typically used for offshore pipelines transporting oil and gas. We consider a J_2-finite strain model expressed in principal stretch form [23], which represents an hyperelastic extension of J_2-flow theory with a standard neo-Hookean model for the elastic part, and nonlinear isotropic hardening with an associative flow rule based on the von Mises yield criterion with isotropic hardening for the plastic part [23]. To model the X65 material a Johnson-Cook nonlinear isotropic hardening rule has been used

$$\sigma_y = A + B e_p^n \tag{44}$$

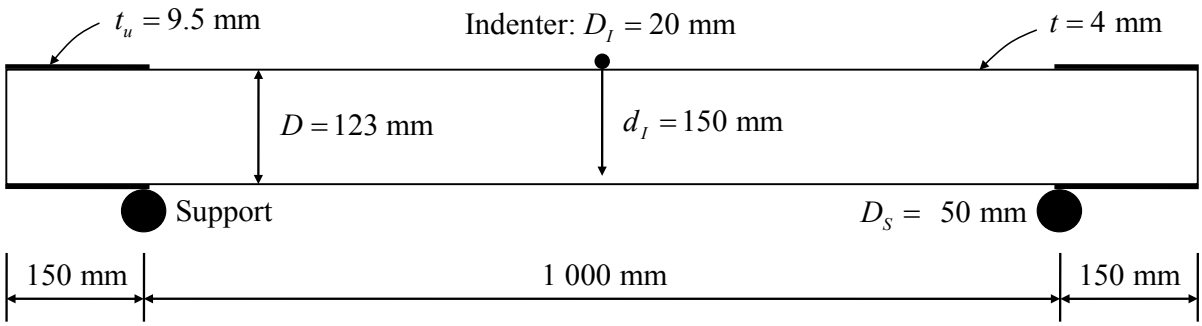

Figure 1: Pipe-impact problem: Geometry and boundary conditions.

where $A = 465.5$, $B = 410.8$ and $n = 0.4793$ are the material parameters obtained from [14] and e_p is the equivalent plastic strain.

Due to symmetry only one quarter of the pipe is modelled as shown in Figure 2a. Both the supports and the indenter are represented by rigid bodies (cylinders). The pipe is analyzed using basis functions of order $p = 2, 3, 4$ for NURBS and $p = 2, 4$ for Lagrange, since for $p = 1$ NURBS and Lagrange approximations coincide. All NURBS and Lagrange discretizations include 48 928 unknowns, one knot-span over the thickness with the highest order NURBS elements, i.e. $n_{cp} = 5$ in the thickness direction and graded in the length and circumferential direction. The different colours of the subdomains shown in Figure 2a indicate that we have subdivided one quarter of the pipe into 10 different patches. We employ a standard Q_p pure displacement formulation for both the NURBS and Lagrange discretizations, with $p+1$ Gauss-Legendre quadrature points in each direction within each knot span/Lagrange element.

Figure 2b shows the L_2-projected mises stress plotted on the deformed configuration for an imposed vertical displacement of the indenter $d_I = 150$ mm, obtained for the quartic order NURBS discretization. Figure 2c shows the corresponding global response represented by the vertical displacement of the top and bottom fiber of the midpoint section of the pipe plotted versus the indenter displacement, while Figure 2d shows the distribution of the equivalent plastic strain over the midpoint cross-section of the pipe at the final load step. The plot of the vertical displacement of the top and bottom fiber demonstrates that the global response is similar for all discretization. Figure 2e shows the local response represented by the maximum equivalent plastic strain versus indenter displacement obtained for the various discretizations. In contrast to the global response the local response deviates for the different discretizations, both for NURBS and Lagrange discretizations. However we observe that the solutions obtained for cubic and quartic order NURBS discretizations coalesce. While for Lagrange solutions we observe oscillations that increase with polynomial order the oscillations for NURBS diminish with increased polynomial order. As a result Lagrange discretizations become stiffer and exhibit convergence problems in the Newton iterations as the polynomial order is increased while for NURBS the smoothness of the contact pressure increases monotonically with the order

of the basis functions. The obtained results stem from the higher degree of smoothness which is achieved by representing the contact geometry by a NURBS surface that is directly inherited from the NURBS discretization of the volume.

Finally, in Figure 2f the contact force between the pipe and the indenter is plotted versus the indenter displacement for all discretizations and compared with the corresponding experimental results [14]. This plot demonstrates the remarkable smoothness obtained with the NURBS discretizations while in contrast the Lagrange solutions are stiffer and experience more oscillations as the polynomial order is increased. Filtering out the dynamic effects from the experimental result the quasi-static solution obtained for the various Lagrange and NURBS discretizations almost coincide with the experiments.

7 CONCLUDING REMARKS

This paper has addressed the application of isogeometric analysis to model frictionless large deformation contact between deformable bodies and rigid surfaces that may be represented by analytical functions. The numerical results show that using NURBS is favorable compared with classical finite elements with Lagrange polynomials as basis functions for a large deformation contact problem involving elastoplastic materials.

The study also reveals that global measures, namely, graphs of displacements or contact forces versus prescribed displacements may be misleading for determining the performance of the element for elastoplastic materials. On the other hand, graphs or contour plots of the distribution of local measures, like the equivalent plastic strain (or von Mises stress), immediately reveal deficiencies of ill-conceived element formulations.

8 ACKNOWLEDGEMENT

The authors acknowledge the financial support from the Norwegian Research Council and the industrial partners of *ICADA*-project; Statoil, Det Norske Veritas and Ceetron, for this work. They also acknowledge the support from the other co-workers in the *ICADA*-project. The first author also would like to acknowledge the support and helpful comments from Professor Laura De Lorenzis, Technische Universität Braunschweig, Germany and PhD Martin Kristoffersen, Structural Impact Laboratory (SIMLab), Centre for Research-based Innovation (CRI), Department of Structural Engineering, Norwegian University of Science and Technology for providing the material data and the experimental results used in this study. Acknowledgements is also made to Dr. Ing. Håvard Ilstad and Dr. Ing. Erik Levold at Statoil ASA for their contributions and for proposing this test case.

REFERENCES

[1] Alart, P. and Curnier, A. A mixed formulation for frictional contact problems prone to Newton like solution methods. *Comput. Meth. Appl. Mech. Engrg.* (1999) **92**:353–375.

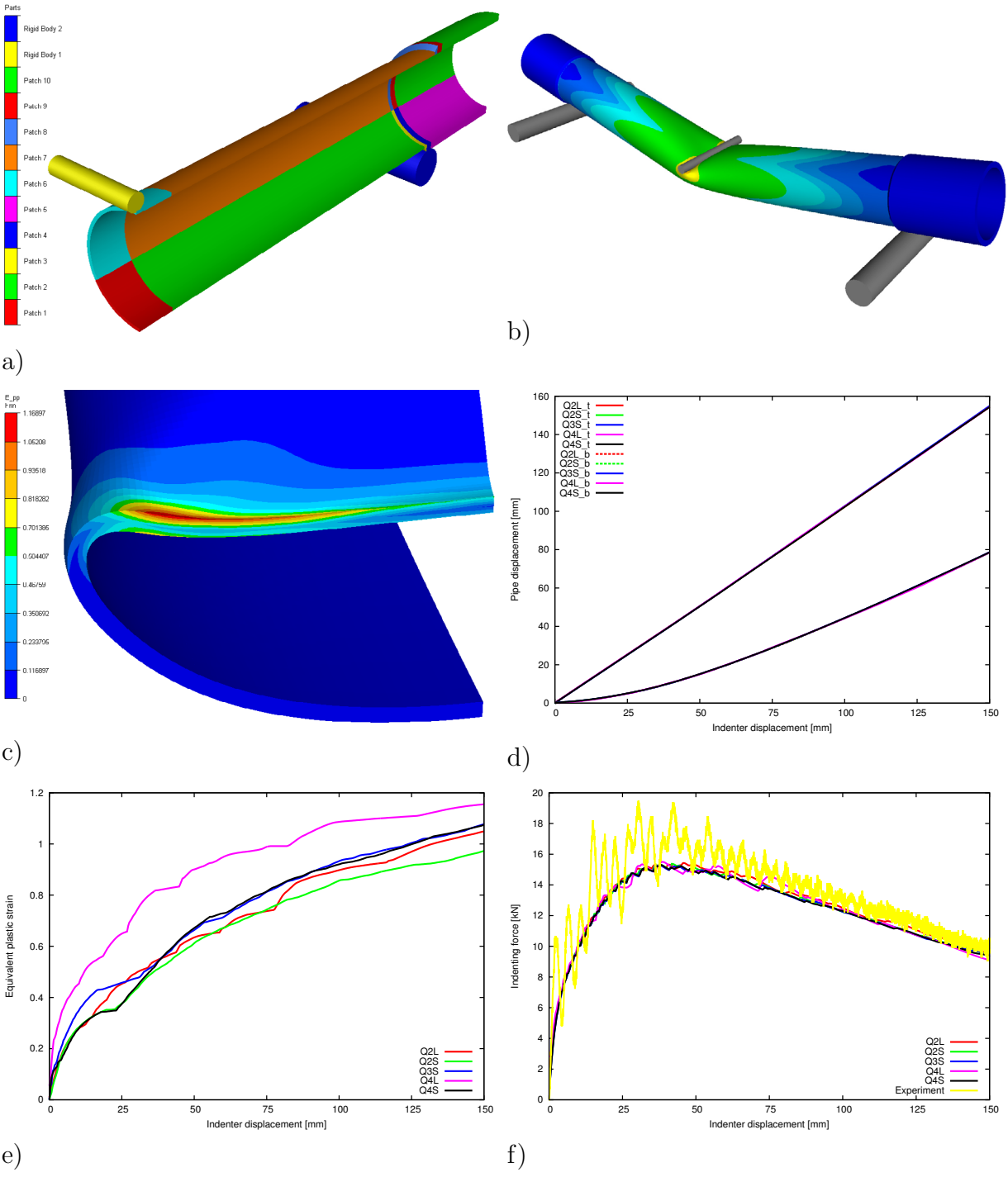

Figure 2: Pipe-impact problem: a) Discretization of a quarter of the problem. b) L_2-projected mises stress plotted on the deformed configuration. c) L_2-projected equivalent plastic strain plotted on the deformed configuration of the midpoint section of the pipe. d) Vertical displacement of the top and bottom fiber of the midpoint section of the pipe. e) Maximum equivalent plastic strain. f) Contact force.

[2] Belgacem, F.B., Hild, P. and Laborde, P. The mortar finite element method for contact problems. *Math. Comp. Model.* (1998) **28**:263–271.

[3] Bergan, P.G. and Mollestad, E. Impact–response behavior of offshore pipelines. *J. Energy-Resour ASME* (1982) **104**:325–329.

[4] Carstens, T., Kjeldsen, S. and Gjørsvik, O. The conflict between pipelines and bottom trawls – some results from laboratory and field tests. *Proc. Offshore North Sea Conference*, Stavanger, Norway (1976) T-I/18:1–28.

[5] Cottrell, J.A., Hughes, T.J.R. and Bazilevs Y. *Isogeometric Analysis: Toward Integration of CAD and FEA*. John Wiley & Sons, Chichester, England, (2009).

[6] Fischer, K.A. and Wriggers, P. Frictionless 2D contact formulations for finite deformations based on the mortar method. *Comput. Mech.* (2005) **36**:226–244.

[7] Gjørsvik, O., Kjeldsen, S.P. and Lund, S. Influences of bottom trawl gear on submarine pipelines. *Proc. 7th Annual Offshore Technology Conference*, Houston (1975) OTC paper 2280:337–345.

[8] Hesch, C. and Betsch, P. A mortar method for energy-momentum conserving schemes in frictionless dynamic contact problems. *Int. J. Numer. Meth. Engrg.* (2009) **77**:1468–1500.

[9] Hüber, S. and Wohlmuth, B.I. A primal-dual active set strategy for non-linear multibody contact problems. *Comput. Meth. Appl. Mech. Engrg.* (2005) **194**:3147–3166.

[10] Hüber, S. and Wohlmuth, B.I. Thermo-mechanical contact problems on nonmatching meshes. *Comput. Meth. Appl. Mech. Engrg.* (2010) **198**:1338–1350.

[11] Hughes, T.J.R., Cottrell, J.A. and Bazilevs, Y. Isogeometric Analysis: CAD, Finite Elements, NURBS, Exact Geometry and Mesh Refinement. *Comput. Meth. Appl. Mech. Engrg.* (2005) **194**:4135–4195.

[12] Hughes, T.J.R., Reali, A. and Sangalli, G. Efficient quadrature for NURBS-based isogeometric analysis. *Comput. Meth. Appl. Mech. Engrg.* (2010) **199**:301–313.

[13] Igland, R.T. and Søreide, T. Advanced pipeline trawl gear impact design. *Proc. ASME 27th International Conference on Ocean, Offshore and Arctic Engineering*, Estoril, Portugal (2008) OMAE2008 paper:271–277.

[14] Kristoffersen, M., Børvik, T., Westermann, I., Langseth, M. and Hopperstad, O.S. Impact against X65 steel pipes – An experimental investigation. *Int. J. Solids. Struct.* (2013) **50**:3430–3445.

[15] Longva, V., Sævik, S., Levold, E. and Ilstad, H. Dynamic simulation of subsea pipeline and trwal board pull-over interaction. *J. Mar. Struct.* (2013) **34**:156–184.

[16] Lorenzis, L.De., Wriggers, P. and Zavarise, G.. A large deformation frictional contact formulation using NURBS-based isogeometric analysis. *Int. J. Numer. Meth. Engrg.* (2011) **87**:1278–1300.

[17] Lorenzis, L.De., Wriggers, P. and Zavarise, G. A mortar formulation for 3D large deformation contact using NURBS-based isogeometric analysis and the augmented Lagrangian method. *Comput. Mech.* (2012) **49**:1–20.

[18] Maaløe, K., Alsos, H.S., and Sævik, S. Detailed analysis of clump-weight interference with subsea pipelines. *Proc. ASME 31th International Conference on Ocean, Offshore and Arctic Engineering*, Rio de Janeiro, Brazil (2012) OMAE2012 paper:725–732.

[19] Mollestad, E. and Bergan, P.G. Nonlinear dynamic analysis of submerged pipelines. *Comput. Meth. Appl. Mech. Engrg.* (1982) **34**:881–891.

[20] Moshagen, H. and Kjeldsen, S.P. Fishing gear loads and effects on submarine pipelines. *Proc. 12th Annual Offshore Technology Conference*, Houston (1980) OTC paper 3782:383–392.

[21] Piegl, L. and Tiller, W. *The NURBS Book*. Springer, Berlin, Germany, 2nd edition, (1996).

[22] Puso, M.A. and Laursen, T.A. A mortar segment-to-segment frictional contact method for large deformations. *Comput. Meth. Appl. Mech. Engrg.* (2004) **193**:4891–4913.

[23] Simo, J.C. and Hughes, T.J.R. *Interdisciplinary Applied Mathematics*, vol.7, Springer, Berlin, Germany, (1998).

[24] Teigen, P., Ilstad, H., Levold, E. and Hansen, K. Hydrodynamic aspects of pipeline overtrawling. *Proc. 19th International Offshore and Polar Engineering Conference.* Osaka, Japan (2009) Paper:435–442.

[25] Temizer, I., Wriggers, P. and Hughes, T.J.R. Contact treatment in isogeometric analysis with NURBS. *Comput. Meth. Appl. Mech. Engrg.* (2011) **200**:1100–1112.

[26] Tur, M., Fuenmayor, F.J. and Wriggers, P. A mortar-based frictional contact formulation for large deformations using Lagrange multipliers. *Comput. Meth. Appl. Mech. Engrg.* (2009) **198**:2860–2873.

[27] Wriggers, P. *Computational Contact Mechanics*. Springer, Berlin, 2nd edition, Germany, (2006).